

Unbiasing Enhanced Sampling on a High-dimensional Free Energy Surface with Deep Generative Model

Yikai Liu,^{*,†} Tushar K. Ghosh,^{*,‡} Guang Lin,^{*,†} and Ming Chen^{*,‡}

[†]*Department of Mechanical Engineering, Purdue University, West Lafayette, IN, 47906*

[‡]*Department of Chemistry, Purdue University, West Lafayette, IN, 47906*

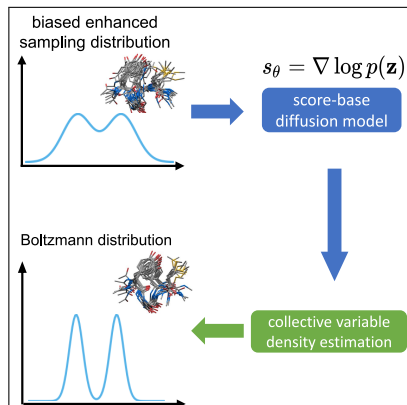
E-mail: liu3307@purdue.edu; tkghosh@purdue.edu; guanglin@purdue.edu; chen4116@purdue.edu

arXiv:2312.09404v2 [cs.LG] 18 Dec 2023

Abstract

Biased enhanced sampling methods utilizing collective variables (CVs) are powerful tools for sampling conformational ensembles. Due to high intrinsic dimensions, efficiently generating conformational ensembles for complex systems requires enhanced sampling on high-dimensional free energy surfaces. While methods like temperature-accelerated molecular dynamics (TAMD) can adopt many CVs in a simulation, unbiasing the simulation requires accurate modeling of a high-dimensional CV probability distribution, which is challenging for traditional density estimation techniques. Here we propose an unbiasing method based on the score-based diffusion model, a deep generative learning method that excels in density estimation across complex data landscapes. We test the score-based diffusion unbiasing method on TAMD simulations. The results demonstrate that this unbiasing approach significantly outperforms traditional unbiasing methods, and can generate accurate unbiased conformational ensembles for simulations with a number of CVs higher than usual ranges.

TOC Graphic



Keywords

Enhanced Sampling, Machine Learning, Score-based Diffusion Model, Molecular Dynamics Simulation

Molecular Dynamics (MD) simulations have emerged as a primary computational tool for studying the thermodynamic and kinetic properties of complex systems in chemistry, biology, and material science.¹ With the assistance of supercomputers,^{2,3} it is now possible to perform milliseconds of all-atom MD simulations for medium-sized proteins. To extend MD simulations to broader time and length scales, multiple enhanced sampling methods have been designed to increase MD sampling efficiency.⁴⁻¹⁴ Among all enhanced sampling methods, CV-based enhanced sampling methods focus on several important degrees of freedom that capture systems’ essential dynamics. By biasing the probability distribution along CVs, CV-based enhanced sampling methods encourage systems to cross high energy barriers and explore different regions of the energy landscape more efficiently.

A critical assumption behind CV-based enhanced sampling methods is the manifold hypothesis,¹⁵⁻¹⁷ which posits that high-dimensional all-atom configurations often lie along a low-dimensional latent manifold, and such a low-dimensional manifold can accurately describe the important features of the high-dimensional systems. Traditionally, physics-based CVs are chosen from experimentally measurable properties, geometric descriptors and order parameters with important underlying physics, such as end-to-end distance,¹⁸ radius of gyration,¹⁹ or backbone torsion angles of proteins.²⁰ Recently, machine-learning-based methods that utilize dimensionality reduction techniques have been applied to design CVs.²¹⁻³² Regardless of CV categories, it is challenging to fully describe a complex system in biochemistry and material science with one or two parameters, a typical number of CVs used in many enhanced sampling simulations. For example, following Two Nearest Neighbors method,³³ we estimate the intrinsic dimension (minimum numbers of parameters) to accurately describe Amyloid-beta 42 ($A\beta_{42}$)³⁴ to be 7.13, as shown in Fig.(1). A number of CVs below 7 will not fully describe this system.

For most enhanced sampling methods³⁵⁻³⁸ that utilize biasing potentials to assist cross-

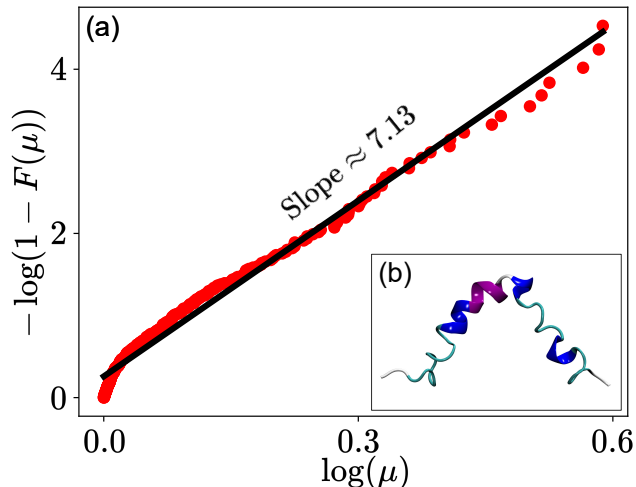


Figure 1: (a) The Two Nearest Neighbors method calculates the ratio μ between the nearest and the second nearest neighbour distance for each data point (red dots). $F(\mu)$ is the cumulative distribution of μ . The slope (black fitting line) of $-\log(1 - F(\mu))$ as a function of $\log(\mu)$ is an estimation of the intrinsic dimension of $A\beta_{42}$ (see the Supporting Information for details of the Two Nearest Neighbors method). (b) The molecular structure of $A\beta_{42}$.

ing of energy barriers, it is challenging to use many CVs, primarily due to the difficulty of constructing accurate biasing potential for a high-dimensional FES. Other methods like driven-adiabatic free energy dynamics/temperature accelerated molecular dynamics (TAMD),^{6,7,35,39} which enhance MD sampling by rising the temperature of certain degrees of freedom, are capable of adopting many CVs in enhanced sampling simulations, since biasing potential is not required. However, when handling many CVs, the task of unbiasing TAMD trajectories to produce unbiased conformational ensembles becomes increasingly complex. This complexity arises from the need for accurate modeling of the high-dimensional, often multimodal CV probability distribution. Traditional density estimation techniques, such as histogram methods, kernel Density Estimation (KDE),⁴⁰ Nearest Neighbor Density Estimation,⁴¹ and Gaussian Mixture Model (GMM),⁴² often struggle to accurately capture the nuances of such intricate distributions. For instance, KDE suf-

fers in high-dimensional spaces as it may produce overly smooth or distorted estimates due to the lack of data across the expansive high-dimensional space. On the other hand, GMM suffers from scalability, initialization sensitivity, and a trivial model selection process. In this paper, we leverage the score-based diffusion model (SBDM)⁴³ for accurate unbiasing of enhanced sampling simulations with many CVs. In our study, we evaluate the performance of the SBDM-based unbiasing method in TAMD simulations. We will demonstrate that SBDM excels in constructing CV probability distributions, and can adapt to non-Euclidean CV such as torsion angles, with minor changes to the model architecture.⁴⁴ These capacities endow the SBDM-based unbiasing method with superior performance and versatility.

We will first introduce the TAMD method and its unbiasing formula. For a system of N particles, we denote its Cartesian coordinates by $\mathbf{r} \equiv (\mathbf{r}_1, \mathbf{r}_2, \dots, \mathbf{r}_N)$, and n collective variables by $\mathbf{q} \equiv (q_1(\mathbf{r}), \dots, q_n(\mathbf{r}))$. In TAMD, \mathbf{q} are coupled with extended variables $\mathbf{z} \equiv (z_1, \dots, z_n)$ with stiff harmonic potentials $\sum_i \kappa_i/2(q_i(\mathbf{r}) - z_i)^2$. \mathbf{z} typically shares the same topology as \mathbf{q} . It has been proved that the free energy surface $A(\mathbf{q})$ can be approximated with the free energy surface of extended variables $A_\kappa(\mathbf{z})$ when $\kappa_i \rightarrow \infty$ for all κ_i . TAMD introduces a high temperature $T_h \gg T$ for \mathbf{z} , and maintains \mathbf{r} at desired temperature T . To keep the thermodynamic properties of the system, \mathbf{z} are adiabatically decoupled from \mathbf{r} by assigning each z_i a fictitious mass $\mu_i \gg 1$. By defining $\beta_h = 1/k_B T_h$ where k_B is the Boltzmann constant, the joint probability distribution of \mathbf{r} and \mathbf{z} from a TAMD simulation satisfies³⁵

$$P_{\text{TAMD}}(\mathbf{r}, \mathbf{z}) \approx P_{T_h}(\mathbf{z})P(\mathbf{r}|\mathbf{z}) , \quad (1)$$

where $P_{T_h}(\mathbf{z}) \propto \exp\{-\beta_h A_\kappa(\mathbf{z})\}$ is the marginal probability distribution of \mathbf{z} and $P(\mathbf{r}|\mathbf{z})$ is the Boltzmann distribution at the physical temperature T conditional on \mathbf{z} . Eq.(1) is exact if all $\mu_i \rightarrow \infty$. The free energy of collective variables $A_\kappa(\mathbf{z})$ can be easily obtained from TAMD with $A(\mathbf{z}) \approx -k_B T_h \log P_{T_h}(\mathbf{z})$.

We are often interested in intuitive features

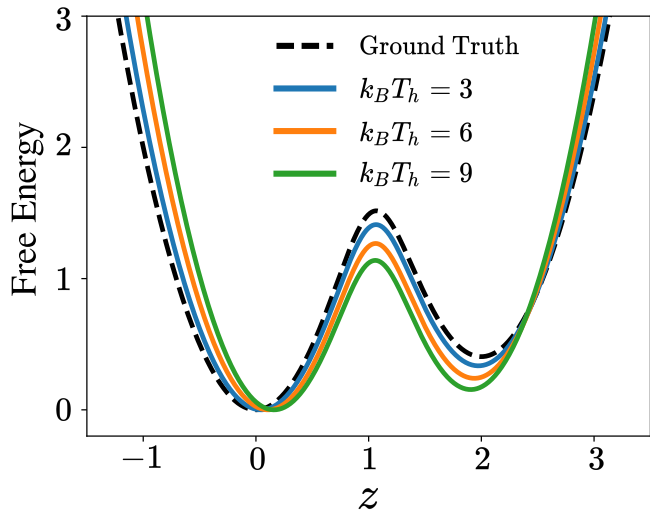


Figure 2: The free energy profiles generated from the unbiasing method of using Eq.(2) are shown as solid lines with an “inaccurate” estimation of the high-temperature probability. The blue, orange, and green lines correspond to unbiasing results from $k_B T_h = 3, 6,$ and 9 , with $k_B T = 1$ in all three cases. The black dashed line is the ground truth with accurate estimation of the high-temperature probability.

that are different from CVs used in an enhanced sampling to understand properties of the simulated system. Unbiasing enhanced sampling trajectories is necessary to project biased simulation data onto intuitive features. Assuming $\mathbf{Y}(\mathbf{r})$ is a set of low dimensional intuitive features of interests, the equilibrium probability of $\mathbf{Y}(\mathbf{r}) = \mathbf{y}$ can be written as

$$P(\mathbf{y}) = \int \delta(\mathbf{y} - \mathbf{Y}(\mathbf{r}))\omega(\mathbf{z})P_{\text{TAMD}}(\mathbf{r}, \mathbf{z})d\mathbf{r}d\mathbf{z}, \quad (2)$$

where $\omega(\mathbf{z}) = P_{T_h}(\mathbf{z})^{T_h/T-1}$ is the unbiasing weight. If \mathbf{Y} can be written as a function of CVs, Eq.(2) can be reduced to $P(\mathbf{y}) = \int \delta(\mathbf{y} - \mathbf{Y}(\mathbf{z}))\omega(\mathbf{z})P_{T_h}(\mathbf{z})d\mathbf{z}$.

A good estimation of $P_{T_h}(\mathbf{z})$ is crucial for obtaining an accurate $\omega(\mathbf{z})$ in TAMD. Errors in estimating $P_{T_h}(\mathbf{z})$ magnify errors in $\omega(\mathbf{z})$ at a high T_h , leading to inaccurate $P(\mathbf{y})$. We design a toy problem to demonstrate the importance of accurately modeling $P_{T_h}(\mathbf{z})$ in unbiasing TAMD. In this example, a one dimensional probability density $P(\mathbf{z})$ at $k_B T = 1$ is constructed with a mixture of Gaussians. The probability is scaled

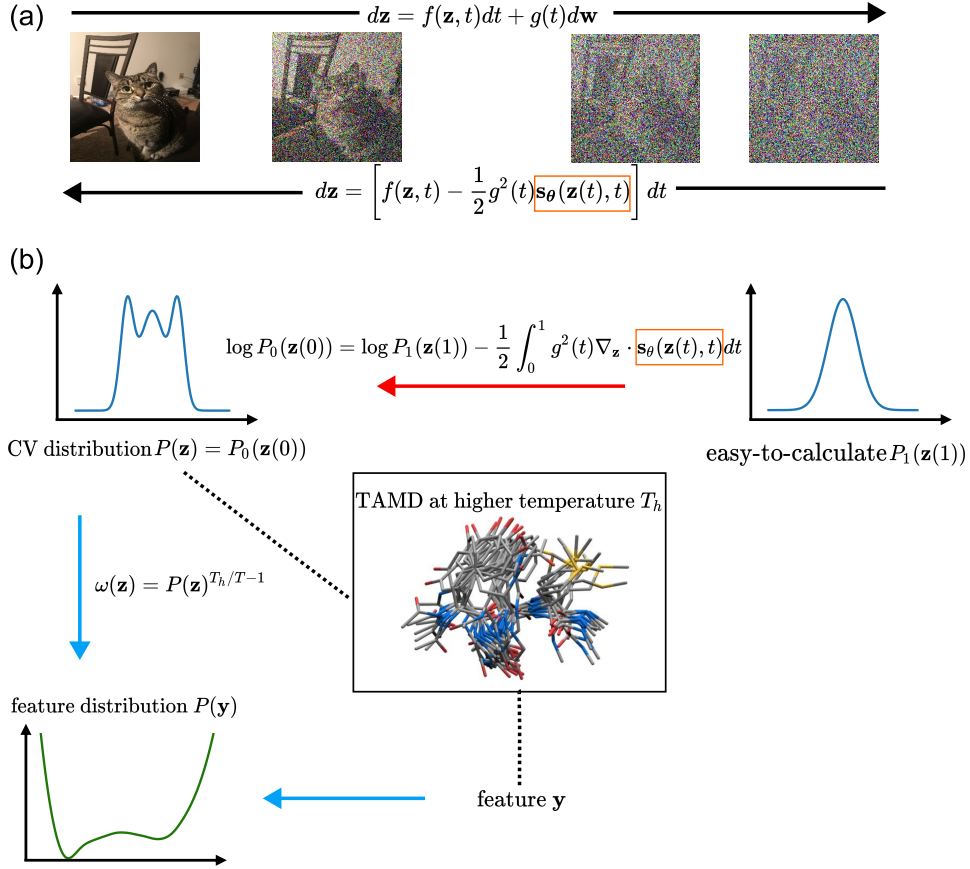


Figure 3: (a) The mechanism of denoising SBDM. During the diffusion process, the data (in this demonstration a picture) is gradually perturbed to an isotropic Gaussian noise via a forward SDE. (b) The flow chat of unbiasing TAMM with SBDM. We perform TAMM simulation at a high temperature T_h , and construct SBDM for \mathbf{z} . The time-dependent score function, squared in orange, is used to perform density estimation of CV, $P(\mathbf{z}) \equiv P_{T_h}(\mathbf{z})$, from a simple distribution, as shown above the red line. The weight $\omega(\mathbf{z})$ of configurations is evaluated from the estimated CV probability $P(\mathbf{z})$. The weight is used to compute the unbiased distribution of features of interest $P(\mathbf{y})$.

to different T_h followed by convolution with a Gaussian kernel to “perturb” the high temperature probability $\tilde{P}_{T_h}(\mathbf{z})$. $\tilde{P}_{T_h}(\mathbf{z})$ is used to calculate weight $\omega(\mathbf{z})$. The “unbiased” distribution of \mathbf{z} , $P_{\text{ub}}(\mathbf{z})$, is then calculated with Eq.(2) (see the Supporting Information for details of the toy problem). Fig.(2) demonstrates that the error in $P_{\text{ub}}(\mathbf{z})$ is more sensitive to errors in $\tilde{P}_{T_h}(\mathbf{z})$ when T_h is higher.

We then briefly review the SBDM framework and its usage in density estimation. The SBDM perturbs data to noise prior with a diffusion process over a unit time by a linear stochastic differential equation (SDE):

$$d\mathbf{z} = f(\mathbf{z}, t)dt + g(t)d\mathbf{w}, \quad t \in [0, 1], \quad (3)$$

where $f(\mathbf{z}, t), g(t)$ are user-defined drift and

diffusion functions of the SDE and \mathbf{w} denotes a standard Wiener process. In this paper, an SDE with the drift term $f(\mathbf{z}, t) = 0$ is used. With carefully designed $g(t)$, the marginal probability of \mathbf{z} at diffusion time t , $P_t(\mathbf{z})$, changes from the data distribution at $t = 0$ to approximately a simple Gaussian distribution at $t = 1$.

For any diffusion process in Eq.(3), it has a corresponding reverse-time SDE⁴⁵ :

$$d\mathbf{z} = [f(\mathbf{z}, t) - g^2(t)\nabla_{\mathbf{z}} \log P_t(\mathbf{z})]dt + g(t)d\bar{\mathbf{w}}, \quad (4)$$

with $\bar{\mathbf{w}}$ a standard Wiener process in the reverse-time. The trajectories of the reverse SDE have the same marginal densities as the forward SDE. Thus, the reverse-time SDE can

gradually convert noise to data. The SBDM parameterizes the time-dependent score function $\nabla_{\mathbf{z}} \log P_t(\mathbf{z})$ in the reverse SDE with a neural network $\mathbf{s}_\theta(\mathbf{z}(t), t)$. To estimate $\nabla_{\mathbf{z}} \log P_t(\mathbf{z})$, a time-dependent score-based model $\mathbf{s}_\theta(\mathbf{z}(t), t)$ can be trained via minimizing a denoising score matching loss:

$$\begin{aligned} M(\theta) &= \left\| \mathbf{s}_\theta(\mathbf{z}(t), t) - \nabla_{\mathbf{z}(t)} \log P(\mathbf{z}(t)|\mathbf{z}(0)) \right\|_2^2 \\ J(\theta) &= \arg \min_{\theta} \mathbb{E}_t \left\{ \mathbb{E}_{\mathbf{z}(0)} \mathbb{E}_{\mathbf{z}(t)|\mathbf{z}(0)} M(\theta) \right\}, \end{aligned} \quad (5)$$

with t uniformly sampled between $[0, 1]$. We note that $\nabla_{\mathbf{z}(t)} \log P(\mathbf{z}(t)|\mathbf{z}(0))$ is not explicitly required in the score matching loss while samples following $P(\mathbf{z}(t)|\mathbf{z}(0))$ are needed.

Finally, SBDM defines a deterministic way to compute the data distribution $P_0(\mathbf{z})$ as follows, with $f(\mathbf{z}, t) = 0$:

$$\begin{aligned} \log P_0(\mathbf{z}(0)) &= \log P_1(\mathbf{z}(1)) \\ &\quad - \frac{1}{2} \int_0^1 g^2(t) \nabla_{\mathbf{z}} \cdot \mathbf{s}(\mathbf{z}(t), t) dt. \end{aligned} \quad (6)$$

CVs can be defined in spaces with different topologies. For example, n torsion angles are defined on a hypertorus space \mathbb{T}^n , and quaternions which representing rigid-body rotation are defined on a 3D unit sphere \mathbb{S}^3 . Therefore, extending the SBDM to different topologies is important. In this study we will focus on SBDM on a hypertorus space. The theory behind SBDM holds for compact Riemannian manifolds, with subtle modifications. For $\mathbf{z} \in M$, a Riemannian manifold (such as hypertorus \mathbb{T}^n), \mathbf{w} being the Brownian motion on the manifold, and $f(\mathbf{z}, t) \in T_{\mathbf{z}}M$, a tangent space, Eq.(4) still holds.⁴⁴

As shown in Eq.(5), training a denoising score matching model requires sampling from the perturbation kernel $P(\mathbf{z}(t)|\mathbf{z}(0))$ of the forward diffusion defined by Eq.(3). We consider the perturbation kernel on \mathbb{T}^n with wrapped normal distribution:

$$\begin{aligned} \mathbf{U}_{\mathbf{d}}(t) &= \frac{\|\mathbf{z}(0) - \mathbf{z}(t) + 2\pi\mathbf{d}\|^2}{2\sigma^2(t)}, \quad \mathbf{d} \in \mathbb{Z}^n \\ P(\mathbf{z}(t)|\mathbf{z}(0)) &\propto \sum_{\mathbf{d}} \exp(-\mathbf{U}_{\mathbf{d}}(t)), \end{aligned} \quad (7)$$

where $g(t)$ and $\sigma(t)$ are related by $g(t) = \sqrt{d\sigma^2(t)/dt}$. The rest of the terms in the loss function in Eq. (5) remain the same. Note

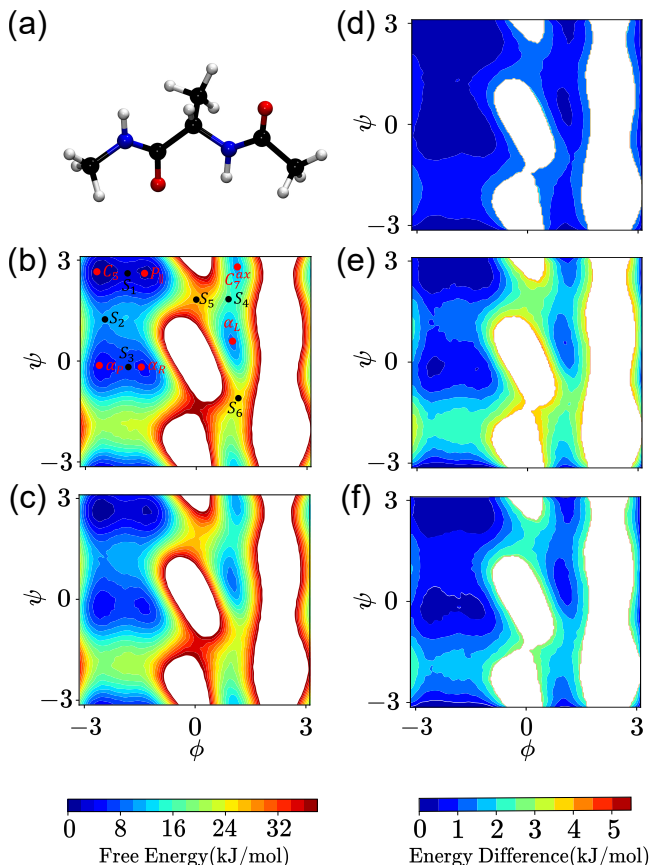


Figure 4: Molecular structure of alanine dipeptide is shown in (a). (b, c) FES w.r.t backbone dihedral angles of alanine dipeptide are presented, obtained by metadynamics (b) and SBDM-TAMD (c). The red/black points represent the location of important minima and saddle points on the FES. (d-f) The absolute free energy difference between metadynamics and SBDM-TAMD, KDE-TAMD, and GMM-TAMD.

that density estimation in Eq.(6) is applicable to both variables in Euclidean and hypertorus space. The architecture of an SBDM model is highly flexible. For example, an SBDM model can use Residual neural network (ResNet),⁴⁶ U-Net,⁴⁷ Graph Neural Network (GNN),⁴⁸ etc.

In the following section, we will demonstrate how incorporating SBDM can fulfill the strict density estimation accuracy requirement of unbiased TAMM, thus allowing TAMM to generate correct unbiased ensembles. We tested

the efficiency and accuracy of SBDM to unbiased TAMD simulations on three systems: (1) alanine dipeptide (2) glutamine dipeptide, and (3) met-enkephalin (see the Supporting Information for simulation details). In all three systems, we conducted TAMD with torsion angles as collective variables, with $T_h = 1200K$ in the first example while $T_h = 900K$ in the second and third examples. The physical variables were maintained at temperature $T = 300K$ in all three experiments. We then unbiased TAMD with density estimation performed by SBDM on hypertorus space (see the Supporting Information for details of training SBDM models). Unbiasing TAMD with SBDM as density estimation method is referred as SBDM-TAMD in the rest of the paper. The general framework of SBDM-TAMD is summarized in Fig.(3). For a fair comparison, we unbiased the same TAMD simulations with kernel density estimation (KDE-TAMD) and Gaussian Mixture Model (GMM-TAMD) in all three systems, and Normalizing Flow on hypertorus space (NF-TAMD)^{49,50} in the last system. We performed converged metadynamics simulations at $300K$ as the baseline results of all three systems. We will compare the unbiased results from different density estimation methods to the baseline results.

The first proof-of-concept example is an alanine dipeptide in the aqueous solution with implicit solvent. This has been a benchmark system with well-established FES in previous studies.^{51,52} In both TAMD and the baseline metadynamics, we used the Ramachandran angles (ϕ , ψ) as CVs. The accuracy of SBDM-TAMD is demonstrated in Fig.(4). The SBDM capably captures the intricate free energy delineated by metadynamics, as shown in Fig.(4)(c) and Fig.(4)(d). Notably, the model accurately locates all six free energy minima, with depth of the minima quantitatively accurate (<1 kJ/mol energy difference). Furthermore, the saddle points - representative of transitional between conformational basins, are also well reproduced. Energy errors in low free energy saddle points are less than 2 kJ/mol compared to metadynamics results. This match implies that the SBDM-TAMD is accurate for studying both

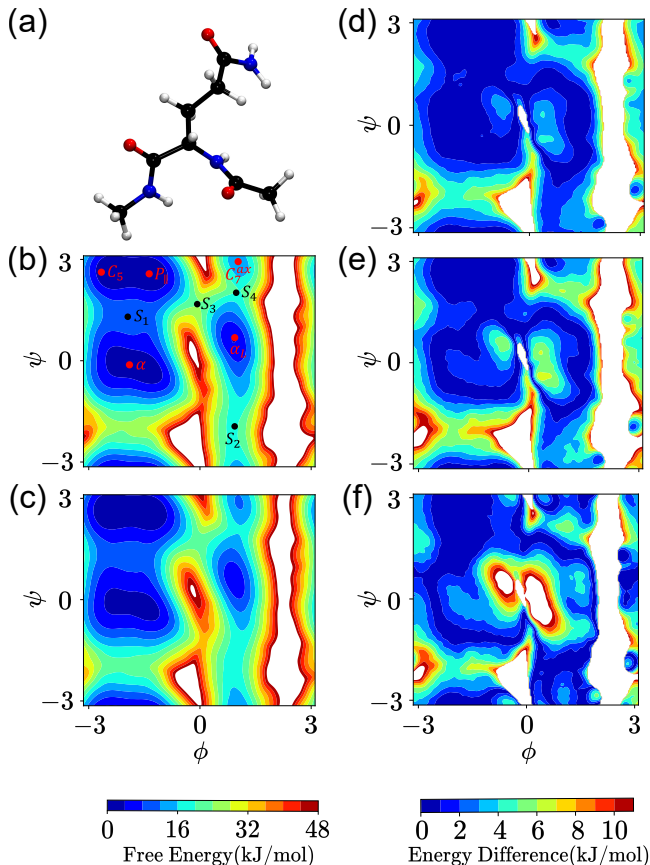


Figure 5: Molecular structure of Glutamine dipeptide is shown in (a). FES of backbone dihedral angles of Glutamine dipeptide are calculated by metadynamics (b) and SBDM-TAMD (c). The red/black points represent the location of important minima and saddle points on the FES. (d)-(f) shows the absolute free energy difference between metadynamics and SBDM-TAMD, KDE-TAMD, and GMM-TAMD.

thermodynamics and kinetics of alanine dipeptide conformational changes. We notice that for this two-dimensional problem, KDE and GMM perform relatively well, but still with less accuracy compared to SBDM. Both methods can locate the free energy minima but with a larger energy difference of up to 2.5 kJ/mol from the baseline metadynamics. The free energy of saddle points have even larger deviation, up to 3.5 kJ/mol. The clear disparities in free energy differences, as shown in Fig. 4(e) and Fig. 4(f), especially in regions corresponding to the annotated energy minima and saddle points, illustrate the inadequacies of KDE and GMM for precise FES calculations.

The second system we studied is Glutamine dipeptide in the aqueous solution with explicit solvent. A TAMD simulation was performed with five dihedral angles on the backbone and the side chain ($\phi, \psi, \chi_1, \chi_2, \chi_3$) as CVs to enhance the sampling of both backbone and side chain conformations. We also run a benchmark metadynamics with two backbone dihedral angles as CVs. The result is demonstrated in Fig.(5). Projecting unbiased SBDM-TAMD trajectory onto backbone dihedral angles quantitatively matches the benchmark FES from metadynamics. Energy errors of minima on the projected 2D FES are within 2 kJ/mol while errors of low-free-energy saddles are approximately 5 kJ/mol. As a comparison, both KDE and GMM struggle to uphold their precision with the increased CV dimensions. Both of these two methods introduce larger errors at α and α_L . This example highlights the SBDM’s superior adaptability and accuracy in high-dimensional CV compared to traditional methods.

The final, more challenging system we studied is the oligopeptide met-enkephalin (Tyr-Gly-Gly-Phe-Met) in the aqueous solution with explicit water, which is a common test case for enhanced sampling techniques.^{35,53,54} For TAMD, we chose ten backbone dihedral angles ($\phi_1, \psi_1, \dots, \phi_5, \psi_5$) as CVs. The baseline metadynamics simulation was performed with a 2D stochastic kinetic embedding (StKE), a manifold learning method which serves as a low-dimensional CV representation that preserves kinetic information.²⁵ We projected the unbiased SBDM-TAMD trajectory to features like end-to-end distance d_{ee} and the radius of gyration R_g . As a comparison, we unbiased the benchmark metadynamics simulation^{55–57} and projected configurations from metadynamics onto the same features. We want to emphasize that generating an optimal machine-learning-based CVs for metadynamics (StKE in this work) is non-trivial and requires extra simulation data. From Fig.(6), the SBDM-TAMD exhibits high performance, demonstrating a FES that closely aligned with the metadynamics baseline. The minima and barriers on each projected one-dimensional FES predicted by SBDM is in good agreements with

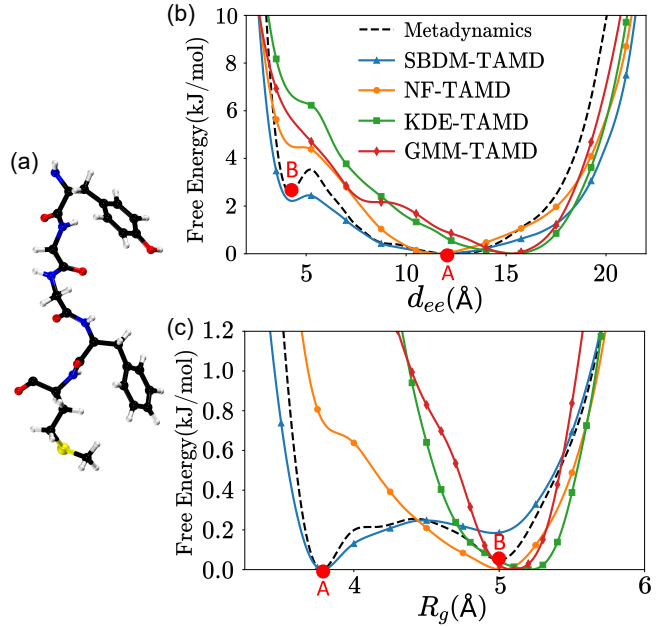


Figure 6: (a) Molecular structure of met-enkephalin. (b-c) Free energy of end-to-end distance and radius of gyration, with red dots indicating stable and meta-stable states.

benchmark, suggesting SBDM-TAMD is capable of modeling thermodynamics and kinetics of a polypeptide. For example, as shown in Fig. 6(b), both metadynamics and SBDM-TAMD identify conformations with small d_{ee} as a meta-stable conformation with consistent meta-stability, while KDE and GMM fail to predict this meta-stable conformation. Also, KDE and GMM fail to predict the location of the global minimum on the FES of d_{ee} with an error of ~ 3.0 Å. Although NF correctly predicts the location of the global minimum, it overestimates the stability of this minimum. Similarly, KDE, GMM, and even NF, predict the most possible $R_g \approx 5$ Å, while SBDM-TAMD predicts that the most stable conformations have $R_g < 4$ Å, which is consistent with the metadynamics’ result.

In this paper, we developed an unbiasing method based on score-based diffusion model, a deep generative learning model, to generate unbiased conformational ensembles from collective-variable-based biased enhanced sampling simulations. Our method can adapt to simulations with collective variables of large amounts and different topologies. We test the

unbiasing method on temperature-accelerated molecular dynamics, an enhanced sampling method that can utilize many collective variables to efficiently explore a high-dimensional free energy surface. Numerical experiments across three systems of 2, 5 and 10 collective variables underscore our unbiasing method’s exceptional accuracy and adaptability to high-dimensional collective variables. Although biomolecules were used in the numerical experiments, the developed approach can be used to other problems like modeling material phase transitions. Looking ahead, we aim to explore the method’s potential in unbiasing simulations with even larger amounts of collective variables, and form accurate high-dimensional biasing potentials for wider ranges of enhanced sampling methods.

Acknowledgement Y.L., T.K.G. and M.C. acknowledge support from Purdue startup funding. G.L. and Y.L. gratefully acknowledge the support of the National Science Foundation (DMS-2053746, DMS-2134209, ECCS-2328241, and OAC-2311848), and U.S. Department of Energy (DOE) Office of Science Advanced Scientific Computing Research program DE-SC0021142, DE-SC0023161, and the Uncertainty Quantification for Multifidelity Operator Learning (MOLUcQ) project (Project No. 81739), and DOE – Fusion Energy Science, under grant number: DE-SC0024583.

Supporting Information Available

Supporting information contains details of MD simulations, SBDM training, Two Nearest Neighbors intrinsic dimension estimation, and toy model.

References

- (1) Ciccotti, G.; Ferrario, M.; Schuette, C., et al. Molecular dynamics simulation. *Entropy* **2014**, *16*, 1.
- (2) Shaw, D. E.; Grossman, J.; Bank, J. A.; Batson, B.; Butts, J. A.; Chao, J. C.; Deneroff, M. M.; Dror, R. O.; Even, A.; Fenton, C. H. et al. Anton 2: raising the bar for performance and programmability in a special-purpose molecular dynamics supercomputer. *SC’14: Proceedings of the International Conference for High Performance Computing, Networking, Storage and Analysis*. 2014; pp 41–53.
- (3) Shaw, D. E.; Adams, P. J.; Azaria, A.; Bank, J. A.; Batson, B.; Bell, A.; Bergdorf, M.; Bhatt, J.; Butts, J. A.; Correia, T. et al. Anton 3: twenty microseconds of molecular dynamics simulation before lunch. *Proceedings of the International Conference for High Performance Computing, Networking, Storage and Analysis*. 2021; pp 1–11.
- (4) Laio, A.; Parrinello, M. Escaping free-energy minima. *Proceedings of the national academy of sciences* **2002**, *99*, 12562–12566.
- (5) Barducci, A.; Bussi, G.; Parrinello, M. Well-tempered metadynamics: a smoothly converging and tunable free-energy method. *Physical review letters* **2008**, *100*, 020603.
- (6) Maragliano, L.; Vanden-Eijnden, E. A temperature accelerated method for sampling free energy and determining reaction pathways in rare events simulations. *Chemical physics letters* **2006**, *426*, 168–175.
- (7) Abrams, J. B.; Tuckerman, M. E. Efficient and direct generation of multidimensional free energy surfaces via adiabatic dynamics without coordinate transformations. *The Journal of Physical Chemistry B* **2008**, *112*, 15742–15757.
- (8) Darve, E.; Rodríguez-Gómez, D.; Pohorille, A. Adaptive biasing force method for scalar and vector free energy calculations. *The Journal of chemical physics* **2008**, *128*, 144120.

- (9) Barducci, A.; Bonomi, M.; Parrinello, M. Metadynamics. *Wiley Interdisciplinary Reviews: Computational Molecular Science* **2011**, *1*, 826–843.
- (10) Abrams, C. F.; Vanden-Eijnden, E. Large-scale conformational sampling of proteins using temperature-accelerated molecular dynamics. *Biophysical Journal* **2010**, *98*, 26a.
- (11) Yu, T.-Q.; Tuckerman, M. E. Temperature-accelerated method for exploring polymorphism in molecular crystals based on free energy. *Physical review letters* **2011**, *107*, 015701.
- (12) Yu, T.-Q.; Chen, P.-Y.; Chen, M.; Samanta, A.; Vanden-Eijnden, E.; Tuckerman, M. Order-parameter-aided temperature-accelerated sampling for the exploration of crystal polymorphism and solid-liquid phase transitions. *The Journal of chemical physics* **2014**, *140*, 214109.
- (13) Samanta, A.; Tuckerman, M. E.; Yu, T.-Q.; E, W. Microscopic mechanisms of equilibrium melting of a solid. *Science* **2014**, *346*, 729–732.
- (14) Tiwary, P.; Parrinello, M. From metadynamics to dynamics. *Physical review letters* **2013**, *111*, 230602.
- (15) Fefferman, C.; Mitter, S.; Narayanan, H. Testing the manifold hypothesis. *Journal of the American Mathematical Society* **2016**, *29*, 983–1049.
- (16) Narayanan, H.; Mitter, S. Sample complexity of testing the manifold hypothesis. *Advances in neural information processing systems* **2010**, *23*.
- (17) Gorban, A. N.; Tyukin, I. Y. Blessing of dimensionality: mathematical foundations of the statistical physics of data. *Philosophical Transactions of the Royal Society A: Mathematical, Physical and Engineering Sciences* **2018**, *376*, 20170237.
- (18) Hummer, G.; Szabo, A. Free energy reconstruction from nonequilibrium single-molecule pulling experiments. *Proceedings of the National Academy of Sciences* **2001**, *98*, 3658–3661.
- (19) Bussi, G.; Gervasio, F. L.; Laio, A.; Parrinello, M. Free-energy landscape for β hairpin folding from combined parallel tempering and metadynamics. *Journal of the American Chemical Society* **2006**, *128*, 13435–13441.
- (20) Granata, D.; Camilloni, C.; Vendruscolo, M.; Laio, A. Characterization of the free-energy landscapes of proteins by NMR-guided metadynamics. *Proceedings of the National Academy of Sciences* **2013**, *110*, 6817–6822.
- (21) Das, P.; Moll, M.; Stamati, H.; Kaviraki, L. E.; Clementi, C. Low-dimensional, free-energy landscapes of protein-folding reactions by nonlinear dimensionality reduction. *Proceedings of the National Academy of Sciences* **2006**, *103*, 9885–9890.
- (22) Ferguson, A. L.; Panagiotopoulos, A. Z.; Debenedetti, P. G.; Kevrekidis, I. G. Integrating diffusion maps with umbrella sampling: Application to alanine dipeptide. *The Journal of chemical physics* **2011**, *134*, 135103.
- (23) Rohrdanz, M. A.; Zheng, W.; Maggioni, M.; Clementi, C. Determination of reaction coordinates via locally scaled diffusion map. *The Journal of chemical physics* **2011**, *134*, 124116.
- (24) Noé, F.; Clementi, C. Kinetic distance and kinetic maps from molecular dynamics simulation. *Journal of chemical theory and computation* **2015**, *11*, 5002–5011.
- (25) Zhang, J.; Chen, M. Unfolding hidden barriers by active enhanced sampling. *Physical review letters* **2018**, *121*, 010601.

- (26) Fu, X.; Xie, T.; Rebello, N. J.; Olsen, B. D.; Jaakkola, T. Simulate time-integrated coarse-grained molecular dynamics with geometric machine learning. *arXiv preprint arXiv:2204.10348* **2022**,
- (27) Ceriotti, M.; Tribello, G. A.; Parrinello, M. Simplifying the representation of complex free-energy landscapes using sketch-map. *Proceedings of the National Academy of Sciences* **2011**, *108*, 13023–13028.
- (28) Tiwary, P.; Berne, B. Spectral gap optimization of order parameters for sampling complex molecular systems. *Proceedings of the National Academy of Sciences* **2016**, *113*, 2839–2844.
- (29) Mendels, D.; Piccini, G.; Parrinello, M. Collective variables from local fluctuations. *The journal of physical chemistry letters* **2018**, *9*, 2776–2781.
- (30) Ribeiro, J. M. L.; Bravo, P.; Wang, Y.; Tiwary, P. Reweighted autoencoded variational Bayes for enhanced sampling (RAVE). *The Journal of chemical physics* **2018**, *149*, 072301.
- (31) Wang, Y.; Ribeiro, J. M. L.; Tiwary, P. Past–future information bottleneck for sampling molecular reaction coordinate simultaneously with thermodynamics and kinetics. *Nature communications* **2019**, *10*, 3573.
- (32) Nuske, F.; Keller, B. G.; Pérez-Hernández, G.; Mey, A. S.; Noé, F. Variational approach to molecular kinetics. *Journal of chemical theory and computation* **2014**, *10*, 1739–1752.
- (33) Facco, E.; d’Errico, M.; Rodriguez, A.; Laio, A. Estimating the intrinsic dimension of datasets by a minimal neighborhood information. *Scientific reports* **2017**, *7*, 12140.
- (34) Findeis, M. A. The role of amyloid β peptide 42 in Alzheimer’s disease. *Pharmacology & therapeutics* **2007**, *116*, 266–286.
- (35) Chen, M.; Cuendet, M. A.; Tuckerman, M. E. Heating and flooding: A unified approach for rapid generation of free energy surfaces. *The Journal of Chemical Physics* **2012**, *137*, 024102.
- (36) Debnath, J.; Parrinello, M. Gaussian Mixture-Based Enhanced Sampling for Statics and Dynamics. *The Journal of Physical Chemistry Letters* **2020**, *11*, 5076–5080, PMID: 32510225.
- (37) Zhang, L.; Wang, H.; E, W. Reinforced dynamics for enhanced sampling in large atomic and molecular systems. *The Journal of Chemical Physics* **2018**, *148*, 124113.
- (38) Zhang, J.; Lei, Y.-K.; Yang, Y. I.; Gao, Y. Q. Deep learning for variational multiscale molecular modeling. *The Journal of Chemical Physics* **2020**, *153*, 174115.
- (39) Cuendet, M. A.; Tuckerman, M. E. Free energy reconstruction from metadynamics or adiabatic free energy dynamics simulations. *Journal of chemical theory and computation* **2014**, *10*, 2975–2986.
- (40) Chen, Y.-C. A tutorial on kernel density estimation and recent advances. *Biostatistics & Epidemiology* **2017**, *1*, 161–187.
- (41) Mack, Y.; Rosenblatt, M. Multivariate k-nearest neighbor density estimates. *Journal of Multivariate Analysis* **1979**, *9*, 1–15.
- (42) Reynolds, D. A., et al. Gaussian mixture models. *Encyclopedia of biometrics* **2009**, 741.
- (43) Song, Y.; Sohl-Dickstein, J.; Kingma, D. P.; Kumar, A.; Ermon, S.; Poole, B. Score-Based Generative Modeling through Stochastic Differential Equations. International Conference on Learning Representations. 2021.
- (44) De Bortoli, V.; Mathieu, E.; Hutchinson, M.; Thornton, J.; Teh, Y. W.;

- Doucet, A. Riemannian score-based generative modelling. *Advances in Neural Information Processing Systems* **2022**, *35*, 2406–2422.
- (45) Anderson, B. D. Reverse-time diffusion equation models. *Stochastic Processes and their Applications* **1982**, *12*, 313–326.
- (46) He, K.; Zhang, X.; Ren, S.; Sun, J. Deep residual learning for image recognition. Proceedings of the IEEE conference on computer vision and pattern recognition. 2016; pp 770–778.
- (47) Ronneberger, O.; Fischer, P.; Brox, T. U-Net: Convolutional Networks for Biomedical Image Segmentation. Medical Image Computing and Computer-Assisted Intervention – MICCAI 2015. Cham, 2015; pp 234–241.
- (48) Scarselli, F.; Gori, M.; Tsoi, A. C.; Hagenbuchner, M.; Monfardini, G. The graph neural network model. *IEEE transactions on neural networks* **2008**, *20*, 61–80.
- (49) Rezende, D. J.; Papamakarios, G.; Racaniere, S.; Albergio, M.; Kanwar, G.; Shanahan, P.; Cranmer, K. Normalizing flows on tori and spheres. International Conference on Machine Learning. 2020; pp 8083–8092.
- (50) Köhler, J.; Krämer, A.; Noé, F. Smooth normalizing flows. *Advances in Neural Information Processing Systems* **2021**, *34*, 2796–2809.
- (51) Strodel, B.; Wales, D. J. Free energy surfaces from an extended harmonic superposition approach and kinetics for alanine dipeptide. *Chemical Physics Letters* **2008**, *466*, 105–115.
- (52) Smith, P. E. The alanine dipeptide free energy surface in solution. *The Journal of chemical physics* **1999**, *111*, 5568–5579.
- (53) Hémin, J.; Fiorin, G.; Chipot, C.; Klein, M. L. Exploring Multidimensional Free Energy Landscapes Using Time-Dependent Biases on Collective Variables. *Journal of Chemical Theory and Computation* **2010**, *6*, 35–47, PMID: 26614317.
- (54) Chen, M.; Yu, T.-Q.; Tuckerman, M. E. Locating landmarks on high-dimensional free energy surfaces. *Proceedings of the National Academy of Sciences* **2015**, *112*, 3235–3240.
- (55) Sutto, L.; D’Abramo, M.; Gervasio, F. L. Comparing the efficiency of biased and unbiased molecular dynamics in reconstructing the free energy landscape of met-enkephalin. *Journal of Chemical Theory and Computation* **2010**, *6*, 3640–3646.
- (56) Sutto, L.; Marsili, S.; Gervasio, F. L. New advances in metadynamics. *Wiley Interdisciplinary Reviews: Computational Molecular Science* **2012**, *2*, 771–779.
- (57) Sicard, F.; Senet, P. Reconstructing the free-energy landscape of Met-enkephalin using dihedral principal component analysis and well-tempered metadynamics. *The Journal of Chemical Physics* **2013**, *138*, 235101.